Effect of rainfall uncertainty on the performance of physically based rainfall–runoff models

Ignacio Fraga[1] **Luis Cea**[2] **Jerónimo Puertas**[2]

[1] CITIC, Department of Mathematics, Universidade da Coruña, A Coruña, Spain

[2] Environmental and Water Engineering Group, Department of Civil Engineering, Universidade da Coruña, A Coruña, Spain

Correspondence
Ignacio Fraga, PhD, CITIC, Department of Mathematics, Universidade da Coruña, A Coruña, Spain.
Email: ignacio.fraga@udc.es

Funding information
European Regional Development Fund; Ministerio de Economía y Competitividad, Grant/Award Number: CGL2013-46245-R; Xunta de Galicia, Grant/Award Number: Centro singular de investigación de Galicia accreditation 2016-2019

Abstract

This paper analyses the effect of rain data uncertainty on the performance of two hydrological models with different spatial structures: a semidistributed and a fully distributed model. The study is performed on a small catchment of 19.6 km^2 located in the north-west of Spain, where the arrival of low pressure fronts from the Atlantic Ocean causes highly variable rainfall events. The rainfall fields in this catchment during a series of storm events are estimated using rainfall point measurements. The uncertainty of the estimated fields is quantified using a conditional simulation technique. Discharge and rain data, including the uncertainty of the estimated rainfall fields, are then used to calibrate and validate both hydrological models following the generalized likelihood uncertainty estimation (GLUE) methodology. In the storm events analysed, the two models show similar performance. In all cases, results show that the calibrated distribution of the input parameters narrows when the rain uncertainty is included in the analysis. Otherwise, when rain uncertainty is not considered, the calibration of the input parameters must account for all uncertainty in the rainfall–runoff transformation process. Also, in both models, the uncertainty of the predicted discharges increase in similar magnitude when the uncertainty of rainfall input increase.

KEYWORDS

distributed and semidistributed hydrological models, GLUE, quantitative precipitation estimation, rainfall uncertainty, rainfall–runoff modelling

1 | INTRODUCTION

The increasing number of physical processes included in operational hydrological models over recent decades, plus advances in the numerical schemes used to solve the model equations, has led to improvements in their performance and range of application. In addition, increases in computational efficiency has allowed the development of more complex models with a high spatial resolution and a very detailed characterization of physical processes (Fraga, Cea, & Puertas, 2017; Goodrich et al., 2012; among others). Enhancements in the capacities of hydrological models has also led to greater concern regarding the accuracy and uncertainty of the input data, due to the decisive impact of these on model predictions (Arnaud, Bouvier, Cisneros, & Dominguez, 2002; Moulin, Gaume, & Obled, 2009).

Rainfall data has been seen as one of the inputs with the greatest impact on model performance (Huard & Mailhot, 2006; Bárdossy & Das, 2008; Beven, 2011). Yet it is also one of the model inputs that presents the highest degree of uncertainty (McMillan, Krueger, & Freer, 2012), this originating mainly from two sources. The first cause of rainfall uncertainty is the result of point measurement errors. Rain gauges represent a reliable way of measuring rainfall depth at a specific location, but they are subject to various kinds of errors (due to mechanical limitations, wind effects, and evaporation losses) that tend to increase with rainfall intensity and sampling frequency (Molini, Lanza, & La Barbera, 2005). The second cause of rainfall uncertainty is

the spatial interpolation at any location from point measurements at a few specific locations. The spatial density of rain gauge networks is rarely sufficient to capture the spatial and temporal variability of the precipitation at small scales (McMillan et al., 2012; Villarini & Krajewski, 2008; Volkmann, Lyon, Gupta, & Troch, 2010). The use of interpolation techniques that combine point and distributed rainfall measurements (i.e., radar or satellite data) partially overcomes this drawback (Bargaoui & Chebbi, 2009; Haberlandt, 2007), but radar and satellite data are not always available at the appropriate temporal and spatial resolutions.

Numerous studies in recent years have focused on characterizing rainfall uncertainty, which is usually quantified either by stochastic perturbation techniques or through conditional simulation methods. In stochastic perturbation methods, the observed rainfall fields are either perturbed with an error function (Pan & Wood, 2009; Turner, Walker, & Oke, 2008) or multiplied by a scale factor (Kavetski, Kuczera, & Franks, 2006; Vrugt, TerBraak, Clark, Hyman, & Robinson, 2008). On the other hand, conditional simulation methods generate multiple replicates of equiprobable rainfall fields (Vischel, Lebel, Massuel, & Cappelaere, 2009). A detailed review of the methodologies used to quantify rainfall uncertainty can be found in McMillan et al. (2012). The development of these methodologies has allowed modellers to include rainfall uncertainty in hydrological computations (Maggioni et al., 2013; Mei, Nikolopoulos, Anagnostou, & Borga, 2016). Prior studies cascaded rainfall uncertainty along rainfall–runoff computations using lumped conceptual models, which ignore the spatial discretization of both the rainfall and the hydrological processes. However, multiple studies have highlighted the sensitivity of hydrological models to the spatial distribution of rainfall and to spatial discretization of the catchment (Fu, Sonnenborg, Jensen, & He, 2011; Shen, Chen, Liao, Liu, & Hong, 2012). Moreover, Haberlandt and Gattke (2004) recognized that the simplicity of the hydrological model can limit the effect of rainfall uncertainty on runoff estimations and recommended the use of physically based distributed models, especially in those catchments subject to adverse weather events with intense and highly variable rainfall. There is, however, an absence of work addressing the effect of rainfall uncertainty on physically based distributed hydrological models and how the spatial structure of rainfall influences estimations of uncertainty.

In this paper, we look at the effect of rainfall uncertainty on the calibration and performance of two hydrological models: a fully distributed and a semidistributed one. The study is carried out in a small catchment located in the north-west of Spain, subject to low pressure fronts generated in the Atlantic Ocean, which produce storm events characterized by a high spatial variability and rainfall intensities. Both hydrological models are calibrated within the generalized likelihood uncertainty estimation (GLUE) framework, using a conditional simulation method to include the uncertainty in rainfall input data. Results show that when rainfall uncertainty is included in the calibration procedure, the uncertainty in the estimation of model parameters is reduced. In addition, the uncertainty bounds on the predicted discharges narrow when the effect of rainfall uncertainty is taken into account in both the calibration procedure and the discharge predictions. This is true for both the fully distributed and the semidistributed models.

2 | STUDY SITE AND DATA

2.1 | Site location

The study site is the catchment of the river Con, located in the north-west of Spain (Figure 1). The catchment has a surface of 19.6 km^2. Despite its relatively small size, the terrain elevation within the catchment varies significantly. The river Con begins at Monte Xiabre (≈650 m asl) and discharges into the sea after crossing the town of Vilagarcia de Arousa. The slopes within the catchment vary from 0.25 m/m near the summit of Monte Xiabre to 0.05 m/m near the catchment outlet.

With a length of 9.6 km, the river Con is the main watercourse along the Con catchment, with two ephemerals discharging to the Con near the town of Vilagarcia. Around two thirds of the watercourse has slopes between 0.01 and 0.03 m/m, whereas the remaining length has a slope of approximately 0.05 m/m. The width of the river

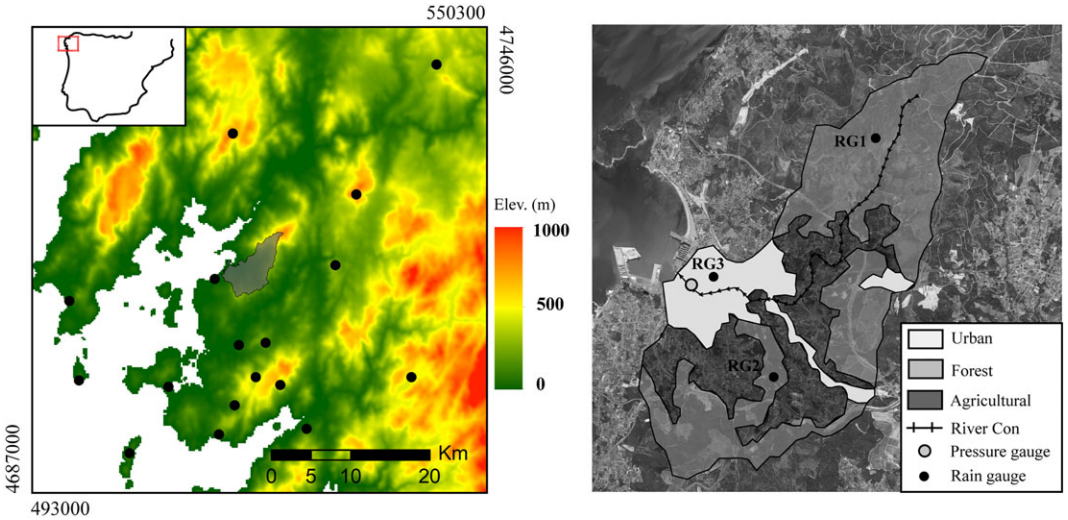

FIGURE 1 A, Study area with the location of the rain gauges used in this study to estimate the uncertainty on the rainfall fields; and B, detail of the Con catchment with the location of the rain gauges used to validate the rainfall predictions and the discharge gauge stations

increases progressively from 0.5 m at the headwater of the river to approximately 3 m at the river discharge.

2.2 | Climate and rainfall

The Con catchment is located in the path of low pressure fronts approaching from the Atlantic Ocean. These fronts are generated at the northern polar regions and are displaced towards the east by the prevailing winds, which dominate at these latitudes. The fronts arriving at the coastline are uplifted due to the sharp topography of the coastal regions. This generates adverse weather events with intense rainfalls characterized by a high spatial and temporal variability (Cabalar-Fuentes, 2005). This behaviour is also observed in other regions, such as the U.S. Pacific Coast, given the similar latitude and orography (Eiras-Barca, Brands, & Miguez-Macho, 2016).

In order to monitor the highly variable rainfall, a dense meteorological network is in place, managed by the regional weather agency MeteoGalicia. The mean annual rainfall registered by the meteorological stations closest to the catchment is approximately 1,300 mm, very similar to the mean value of the region (1,280 mm; MeteoGalicia, 2017).

2.3 | Geology, soil properties, and land use

Three main land uses within the catchment (Figure 1) were identified from the Corine Land Cover raster, provided by the Land Monitoring Core Service of Copernicus. Forest covers approximately 55% of the catchment. These include mainly broad-leaved species, with only a small part (<10% of the total forest surface) of coniferous species. Agricultural land represents 30% of the catchment surface, mainly corn fields with very irregular cultivation patterns. Discontinuous urban fabric represents the remaining 15% of the catchment surface.

Geological data of the catchment was obtained from the GEODE cartographical series, produced by the Spanish National Mining and Geological Institute, whereas soil-related information was obtained from the soil property cartography produced by the University of Santiago (http://rgis.cesga.es/index.html). The soil of the Con catchment is composed of fractured granite, which provides a relatively permeable substrate. The soil density is around 0.75 g/cm^3 in the forest areas and close to 1 g/cm^3 in the urban and agricultural lands. Soil porosity is relatively uniform across the whole catchment, with values at around 60%. Forest lands are mainly composed of sand (70%) with small amounts of silt (10%) and clay (20%). Compared with the forest, agricultural, and urban lands present a lower percentage of sand (50%), a similar content of clay (20%), and a higher silt percentage (30%). Following the United States Department of Agriculture (USDA) texture classification, forest lands correspond to sandy loam soil, whereas agricultural and urban soils correspond to loam soils.

2.4 | Rainfall and discharge data

Seventeen tipping-bucket stations operated by MeteoGalicia were identified in a radius of 50 km around the Con catchment (Figure 1). Rain data from these stations were used to estimate the spatial and temporal distribution of rainfall during 10 storm events registered over the years 2015 and 2016 and to quantify rainfall uncertainty as described in Section 3.2. The characteristics of the rain events are detailed in Table 1. The measuring accuracy of the pluviometers is 0.2 mm, and the time resolution of the observed data is 10 min. Despite the fact that MeteoGalicia operates a meteorological radar, its data were not considered in the present study because they were unavailable for most of the analysed rain events.

In order to validate the predictions obtained from the MeteoGalicia network, three additional pluviometers were installed in the Con catchment during this study, at locations RG1, RG2, and RG3 (Figure 1). The elevations of these pluviometers are 150, 30, and 5 m asl, respectively. These rain gauges have the same measuring and time resolutions as the ones operated by MeteoGalicia.

As noted by several authors (Ciach, 2003; Molini et al., 2005; Villarini, Mandapaka, Krajewski, & Moore, 2008), the accuracy of the tipping-bucket rain gauges increases with the accumulation of time, and the use of these devices for temporal scales lower than 10 min is usually inappropriate (Habib, Krajewski, & Kruger, 2001). For this reason the rainfall depths measured with a 10-min resolution were aggregated to a 30-min interval.

Discharges at the catchment outlet were used to calibrate the hydrological models and to validate the predictions of these. A pressure gauge that monitors the water level was installed 1.2 km upstream the discharge of the Con river into the sea. This location prevents the measured levels being conditioned by the tidal level. The drainage surface at the pressure gauge represents approximately 95% of the catchment surface. The pressure gauge has an accuracy of ±0.1% field scale, a measuring range of 0–2 m, and a sampling frequency of 10 min. Water depths were converted to discharge using a rating curve, which was previously calibrated.

3 | METHODOLOGY

3.1 | Workflow and general description of the methodology

In order to analyse the effect of rainfall uncertainty on the performance of physically based rainfall–runoff models, the first step was

TABLE 1 Characteristics of the analysed rain events. I_{max} and σ_I correspond to the maximum rainfall intensity and the rainfall intensity standard deviation registered at rain gauge RG3 using an aggregation time step of 30 min

Event	Duration (hr)	$I_{max,30min}$ (mm/hr)	σ_I (mm/hr)	Total rainfall depth (mm)
E1	23	5.00	1.11	58.20
E2	5	5.20	1.60	17.00
E3	5	5.20	1.85	16.40
E4	21	8.80	1.77	53.60
E5	11	4.00	1.08	23.60
E6	7	14.00	3.70	24.40
E7	14	3.40	0.76	15.60
E8	11	15.80	3.94	33.40
E9	14	15.80	3.76	33.40
E10	16	7.80	2.28	33.00

to characterize the uncertainty of the estimated rainfall fields during a series of storm events (Section 3.2). Once the rainfall had been characterized, fully distributed and a semidistributed hydrological models of the catchment were made (Sections 3.3 and 3.4). Both hydrological models were calibrated against the river discharge observations at the catchment outlet, using the estimated rainfall fields as input data (Section 3.5). A sensitivity analysis was also performed, in order to better understand the effect of rainfall uncertainty on model calibration (Section 3.6). Finally, the performance of the hydrological models was analysed by comparing the model predictions with the observed hydrographs at the catchment outlet (Section 3.7).

3.2 | Rainfall estimation and uncertainty quantification

Rain data from the MeteoGalicia meteorological stations referred in Section 2.4 was used to interpolate the spatial distribution of rainfall over the Con catchment during the rain events detailed in Table 1. The rainfall fields were interpolated with a spatial and temporal resolution of 250 m and 30 min, respectively. The interpolation was done with the ordinary kriging method, which computes the rainfall depth at any location as a weighted average of the rainfall depths observed at the pluviometers. The weight of each pluviometer is obtained from a variogram function. The variogram is computed for each individual rainfall event from the accumulated rainfall depths during the whole event observed at all the available rain gauges (Delrieu et al., 2014).

The uncertainty of the interpolated rainfall fields was quantified with the conditional simulation method proposed by Lebel, Bastin, Obled, and Creutin (1987) and modified by Vischel et al. (2009). This technique consists of generating multiple error fields for an observed rain event. Here, we have generated five random error fields for each time step of each rain event. A more statistical representation of the uncertainty would be obtained if more random fields were generated, but the computational burden of the simulations performed by the hydrological model made this unfeasible.

The accuracy of the rainfall interpolations and the uncertainty quantification performed following the described procedure was evaluated with the observed rainfall data at the three pluviometers installed within the catchment (RG1, RG2, and RG3 in Figure 1).

3.3 | Hydrological models

Two physically based hydrological models were used to compute the rainfall–runoff transformation and the flow routing in the selected storm events: a fully distributed model and a semidistributed model.

3.3.1 | Fully distributed hydrological model

The distributed hydrological model used in this paper is based in the overland flow model Iber (Bladé et al., 2014; García-Feal et al., 2018), which solves the 2D shallow water equations, coupled to a groundwater flow model, which solves the 2D Boussinesq equations (Cea et al., 2015). The model has been validated in previous studies under conditions of overland flow including rainfall–runoff transformation at different spatial scales (Cea & Bladé, 2015; Cea, Legout, Darboux, Esteves, & Nord, 2014).

The distributed model discretizes the whole catchment in relatively small cells. In this case, the catchment was discretized in 19,321 triangular elements, with sizes ranging from 15 m in the main stream network to 100 m in the hillslopes. The elevation of each element was interpolated from a 5-m DEM provided by the Spanish National Geographical Institute.

The soil properties and land uses (surface roughness, permeability, and porosity) and its hydrological state (water depth, rain intensity, and infiltration rate) vary from one cell to another. The land use assigned to each cell was obtained from the 100-m resolution raster of the Corine Land Cover raster, provided by the Land Monitoring Core Service of Copernicus. In the simulations performed in this study, evapotransporation losses have not been taken into account, because their impact in short and intense storm events is low. Infiltration losses were estimated using a constant potential infiltration rate. Although this simplification ignores the temporal variation of the potential infiltration rate, it can give an acceptable approximation of the average infiltration during short rain events. This approach requires fewer input parameters than other formulations, which avoids overparameterization. Three types of soils with different infiltration parameters are considered in the model (agricultural, forest, or sparse urban).

3.3.2 | Semidistributed hydrological model

The semidistributed model used in this study is version 4.2.1 of HEC-HMS (Scharffenberg & Fleming, 2006). The model lumps the hydrological variables and physical parameters of the catchment into subbasins with spatially homogeneous properties. Rainfall–runoff is computed within each subbasin, and the resulting discharges are routed through the river network to the catchment outlet.

The HEC-GeoHMS software (Fleming & Doan, 2009) was used to discretize the catchment in subbasins. Each subbasin was defined in such a way that it comprises only one of the three land uses (agricultural, forest, or sparse urban). This resulted in 16 subbasins with sizes ranging from 0.2 to 5 km^2. The average terrain elevation and slope of each subbasin was obtained from the same DEM used in the distributed model. In all the subbasins, rainfall–runoff transformation was computed with the Soil Conservation Service (SCS) Unit hydrograph method. The concentration time of each subbasin (Table 2) was determined from the TR55 equations (USDA, 1986). Infiltration losses were evaluated using a constant infiltration rate, and the baseflow was computed using a nonlinear Boussinesq model. Flow routing along the river network was computed using the kinematic wave equation.

3.4 | Models parameters and calibration

Six input parameters were considered for both hydrological models: the hydraulic conductivity and porosity of the soil, the potential infiltration rate of each kind of land use (urban, agricultural, and forest), and the river Manning coefficient (Table 3). The hydraulic conductivity and the porosity of the soil were assumed to be homogeneous in the whole catchment. The potential infiltration rates vary from one subbasin to

another depending on the land use of these. The river's Manning coefficient is the same for the whole stream network. It is important to note here that both models use the same six input parameters, even if their mathematical structure and equations are different.

The parameters of the hydrological models shown in Table 3 were calibrated within the well-established GLUE framework (Beven & Binley, 1992). The GLUE methodology has been successfully applied to the calibration of hydrological models, including semi and fully distributed models, such as the ones used in this paper (Blasone et al., 2008; Shen et al., 2012; Cea, Legout, Grangeon, & Nord, 2016; Fraga et al., 2016; Lehbab-Boukezzi, Boukezzi, & Errih, 2016).

The parameters shown in Table 3 were sampled using the Latin hypercube sampling (LHS) technique. This technique has been successfully used for model calibration in many hydrological studies (Zhao, Chen, Wang, & Tong, 2012; Kim et al., 2015; Fraga et al., 2016). The ranges of variation of the three potential infiltration rates, the soil porosity, and the river's Manning coefficient, were estimated from the HEC-HMS reference manual (Scharffenberg & Fleming, 2006). The range of variation of the hydraulic conductivity of the soil was defined from the values recommended by the U.S. Soil Conservation Service (USDA, 1986).

Regarding the Manning coefficient of the hillslopes, values of 0.15, 0.25, and 0.55 s $m^{-1/3}$ were imposed on the mesh cells (in the distributed model) and subbasins (in the semidistributed model) with urban, agricultural, and forest land uses, respectively. These values were selected from the ones recommended by the U.S. Soil Conservation Service (USDA, 1986) for sheet flow over each type of soil.

In order to limit the computational burden of the simulations, 200 parameter sets were sampled with the LHS technique. For each storm event, the hydrological models were run with the 200 parameter sets, and the performance of each set was evaluated using the following likelihood function:

$$w_j = \frac{\Sigma_{i=1}^{i=N} w_{ij}}{N} \qquad w_{ij} = 1 - \frac{q_1^* - q_{ij}}{\sigma_i} \quad \text{If} \left| q_1^* - q_{ij} \right| < \sigma_i \qquad w_{ij} = 0 \quad \text{If} \left| q_1^* - q_{ij} \right| > \sigma_i, \tag{1}$$

TABLE 2 Characteristics of the subbasins of the semidistributed model

Subbasin	Area (m2)	Slope (%)	Land use	Tc (min)
1	105,672.603	26.04	Forest	60.43
2	5,701,168.78	25.80	Agricultural	56.04
3	1,132,333.93	26.10	Forest	31.38
4	251,642.169	19.86	Sparse urban	31.55
5	1,756,421.65	18.50	Forest	40.65
6	221,289.645	19.00	Agricultural	34.06
7	133,141.264	14.31	Agricultural	16.24
8	766,821.151	14.03	Forest	53.47
9	835,881.921	14.03	Agricultural	48.80
10	783,708.735	7.79	Sparse urban	38.65
11	166,245.259	18.89	Sparse urban	46.79
12	1,569,502.37	16.00	Forest	55.03
13	455,269.442	18.50	Agricultural	49.06
14	362,468.888	8.56	Sparse urban	27.29
15	2,000,995.19	13.70	Forest	107.92
16	3,357,437	13.60	Agricultural	100.68

TABLE 3 Hydrological model input parameters and corresponding ranges of variation considered in their calibration

Symbol	Parameter	Range	Units
k	Hydraulic conductivity	0.05–0.20	m/hr
P	Porosity	0.2–0.6	%
n_R	River Manning coefficient	0.02–0.4	s $m^{-1/3}$
I_U	Infiltration rate sparse urban soil	0–10	mm/hr
I_A	Infiltration rate agricultural soil	2–20	mm/hr
I_F	Infiltration rate forest soil	2–30	mm/hr

where w_j is the likelihood of the jth parameter set and q_i^* and q_{ij} are respectively the observed and computed discharges of the jth simulation at the ith time step, N is the number of time steps over the rain event, and σ_i is the expected standard error of the observed discharge at each time step. The expected error of the observed discharge (σ_i) was assumed as ±10% of the average discharge. This value is within the range proposed by Pelletier (1988) and McMillan et al. (2012) for discharges obtained from stage measurements combined with rating curves. Equation 1 is similar to the performance measure described in Pappenberger and Beven (2004), which also considers the expected observation error in the definition of likelihoods.

Equation 1 gives the likelihood of each parameter set for each storm event. The global likelihood of each parameter set was obtained by multiplying these event-based likelihoods. By multiplying the likelihoods obtained for all the events rather than averaging them, the weight of the parameter sets with a good performance in all the events is increased. Due to the limited number of simulations performed, this constrained by the computational burden of the models, no likelihood threshold was defined. All the simulations were considered behavioural and therefore taken into account during both the calibration and the validation of the hydrological models.

At a first stage, the hydrological models were calibrated without taking into account the uncertainty of the rainfall estimations. The rainfall fields interpolated using the ordinary kriging technique were used as input of the hydrological models. At a second stage, the calibration was repeated including the uncertainty of the rainfall estimations, computed with the conditional simulation method. As noted in previous sections, five equiprobable rain events were used as model inputs. This represents, for each of the two hydrological models, 1,200 simulations per event: 200 simulations with each parameter set for each of the five equiprobable rainfall fields and another 200 simulations using the kriged rainfall fields without uncertainty.

3.5 | Sensitivity analysis

The sensitivity of the output of the models to their input parameters was evaluated using the variance-based Sobol sensitivity indices (Saltelli et al., 2008). Combined with nonparametric metamodels, Sobol sensitivity indices can give a good approximation of model sensitivity even from a very limited number of simulations, and are therefore especially suitable for computationally demanding models (Cea, Bermúdez, & Puertas, 2011; Saltelli et al., 2008; Sobol, 1998). In particular, we analysed the sensitivity to the input parameters of the relative mean

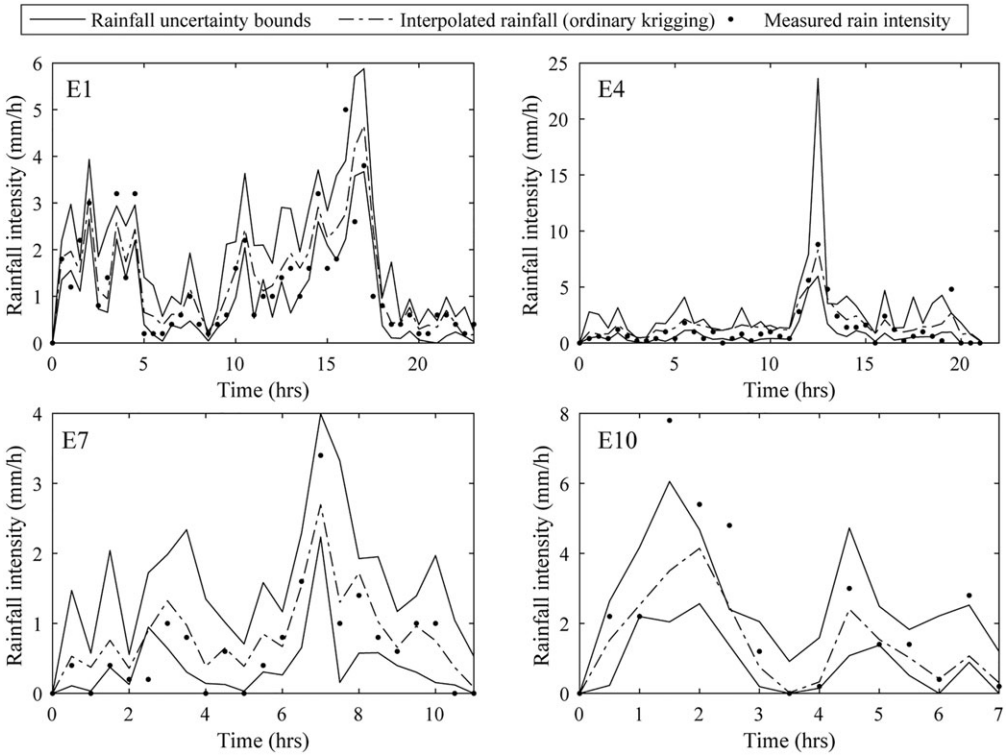

FIGURE 2 Predicted and measured hyetographs at the rain gauge RG3

square error (RMSE), which is a performance measure widely used in hydrology (Legates & McCabe, 1999). The sensitivity indices were computed independently for each rain event from the results of the simulations performed using both the kriged rainfall fields without considering uncertainty and the rainfall fields obtained with the conditional simulation technique to include uncertainty effects.

3.6 | Model validation

A cross-validation procedure was followed to validate the hydrological models. The input parameters were calibrated using nine rain events, and the remaining event was used to validate the model predictions. This was repeated 10 times, discarding one different event at each time. This procedure reduces the effect of the selected calibration data on the validation of the model (Zheng et al., 2018). Uncertainty bounds on the predicted hydrographs were defined from the global likelihood of each parameter set obtained in the GLUE calibration. In order to analyse the effect of rainfall uncertainty on model performance, the validation was done with and without considering the uncertainty in the rainfall fields.

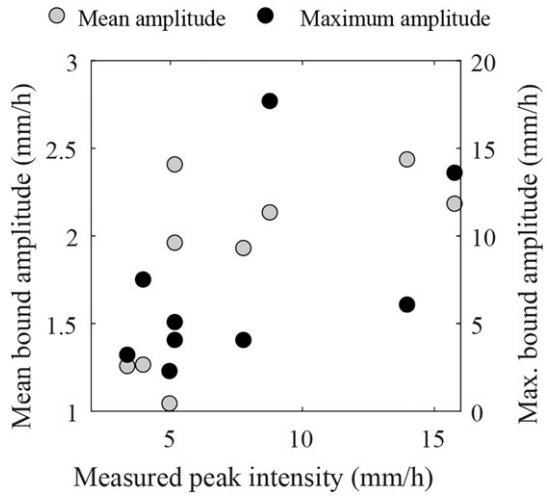

FIGURE 3 Mean and maximum uncertainty amplitudes of the rainfall predictions at the rain gauge RG3

TABLE 4 Percentage of experimental rain data within the 95% confidence interval and confidence interval amplitude at each rain gauge

	Experimental rain data within 95% confidence interval (%)			Mean 95% confidence interval amplitude (mm/hr)		
Event	RG1	RG2	RG3	RG1	RG2	RG3
E1	65*	n.a	67	0.89	1.03	1.03
E2	80*	80*	80*	1.74	2.33	2.38
E3	30*	30	50	1.51	2.09	1.95
E4	57*	69*	69*	1.86	2.63	2.09
E5	55*	64*	68*	0.90	1.36	1.21
E6	57*	29	43	2.67	2.45	2.29
E7	82*	64*	73*	1.14	1.24	1.25
E8	44*	38*	44	2.57	2.58	2.13
E9	11	6	17	2.61	1.94	2.11
E10	na	43	64	1.77	2.33	1.92

*Indicates that the measured peak rain intensity lies within the confidence interval.

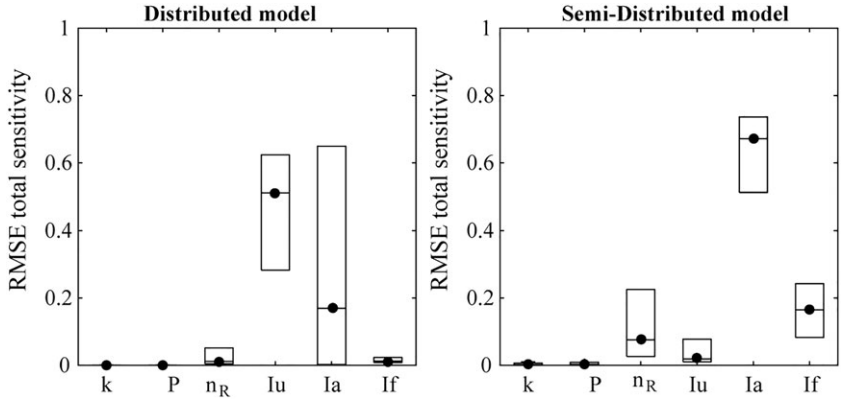

FIGURE 4 Total sensitivity indices of the RMSE to the hydraulic conductivity (k), porosity (P), manning coefficient of the river (n_R) and infiltration rates of the sparse urban (I_U), agricultural (I_A), and forest (I_F) soils. Dots indicate the median values and the bars extend to the 95% confidence interval

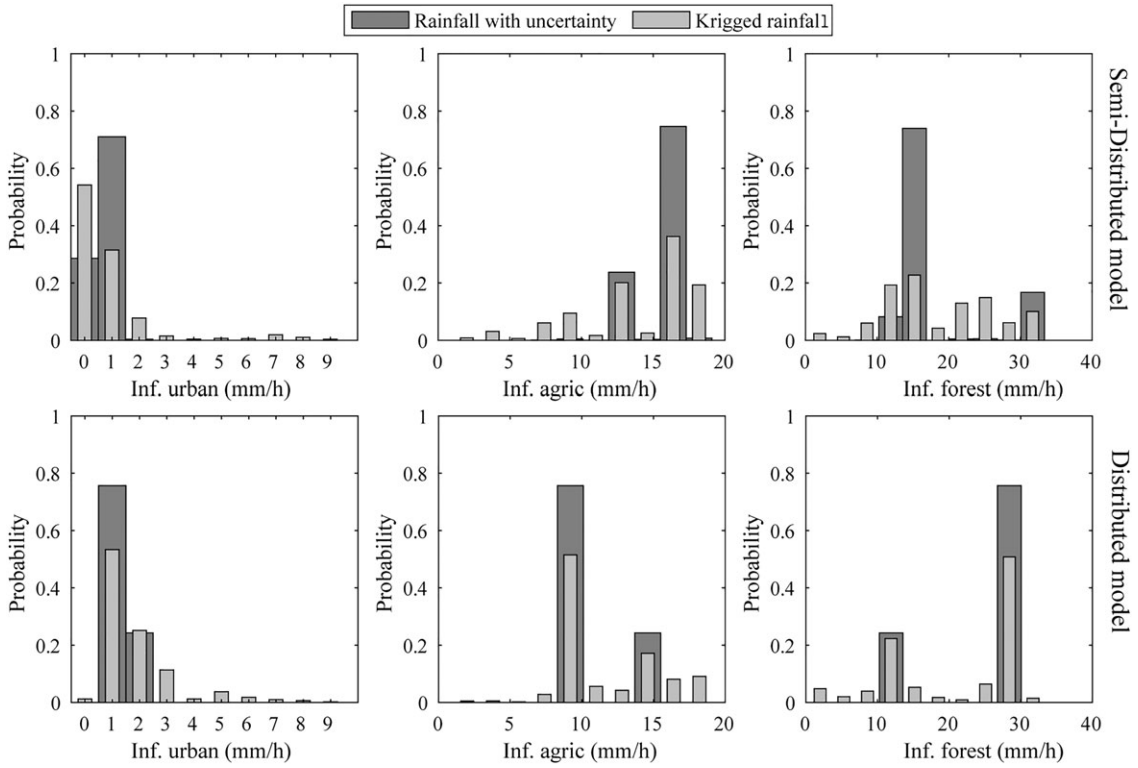

FIGURE 5 Probability distributions of the infiltration rates. Light grey bars show the result of the calibration performed without taking into account rain uncertainty. Dark grey bars correspond to the calibrations performed including the rainfall uncertainty

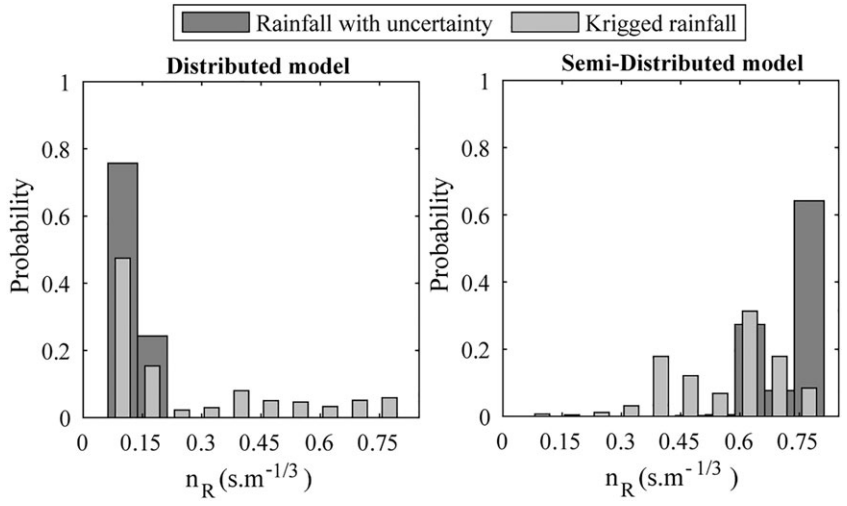

FIGURE 6 Probability distributions of the river manning coefficient. Light grey bars show the result of the calibration performed without taking into account rain uncertainty. Dark grey bars correspond to the calibrations performed including the rainfall uncertainty

TABLE 5 Percentage of experimental discharge data within the 95% confidence interval computed with (RU) and without (NRU) rainfall uncertainties

	Percentage of experimental discharge data within uncertainty bounds (%)			
	Distributed model		Semidistributed model	
Event	RU	NRU	RU	NRU
E1	45*	67*	15	88*
E2	49*	51*	30	77*
E3	36	38	15	10
E4	46	68*	31*	77*
E5	56*	62*	51*	77*
E6	15*	25	15	22*
E7	35	49	63	78*
E8	57*	51*	39*	58*
E9	36	73*	68*	76*
E10	41	48	48	53

*Indicates that the measured peak discharge lies within the confidence interval.

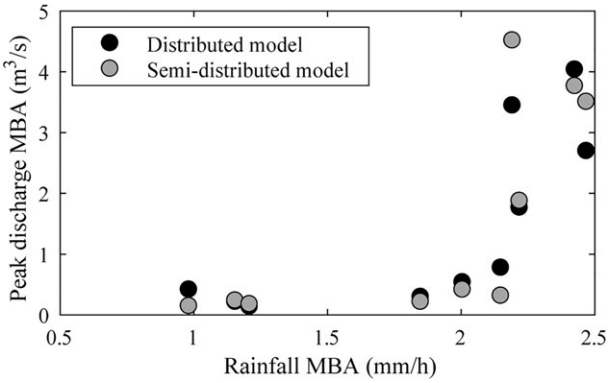

FIGURE 7 Mean bound amplitude (MBA) of the 95% confidence interval of the rainfall and discharge predictions

4 | RESULTS

4.1 | Rainfall interpolation and uncertainty quantification

The comparison between the interpolated and measured rainfall at the validation rain gauge RG3 shows significant differences between rain events (Figure 2). In some events (i.e., E1 and E4), the hyetograph kriged from the measurements of the nearby rain gauges correctly reproduces the observed rainfall. However, in other events (i.e., E10), the shape and peak of the observed hyetographs are not correctly reproduced by the kriged rainfall.

The uncertainty of the interpolated rainfall increases with rain intensity. Both the mean and the maximum bound amplitudes are higher in the events in which the peak rain intensity is highest (Figure 3). The mean amplitude of the uncertainty bounds varies between 15% and 30% of the maximum intensity observed during the rain event. Within each event, the performance observed in the three validation gauges (RG1, RG2, and RG3) is similar, which suggests that the performance of the methodology used to estimate rainfall uncertainty is similar in the whole catchment (Table 4). This conclusion might be expected, given the relatively small size of the catchment.

The observed rain data lying within the uncertainty bounds exceeds 50% in most of the events. The peak rainfall intensity is in general correctly reproduced. In all the storm events except two (Events E9 and E10), the peak rain intensity measured at least at one rain gauge lies within the uncertainty bounds.

4.2 | Sensitivity analysis and model calibration

The total sensitivity indices indicate that the potential infiltration rates have a major impact on the output of both the fully distributed and the semidistributed models (Figure 4). The almost null sensitivities of model outputs to the hydraulic conductivity and the porosity of the soil suggest that the groundwater flow has a negligible effect on the outlet hydrograph. This means that in the study, catchment the groundwater flow parameters might take any value within the considered ranges of variation without affecting the predicted discharges.

TABLE 6 Mean predicted discharges at the catchment outlet computed with (RU) and without (NRU) rainfall uncertainties. Results in brackets correspond to the amplitude of the 95% confidence interval

	Mean predicted peak discharge (m^3/s)				
	Distributed model		Semidistributed model		Measured peak discharge (m^3/s)
Event	RU	NRU	RU	NRU	
E1	2.44 (0.41)	1.9 (0.92)	1.31 (0.14)	1.35 (0.95)	2.08
E2	1.87 (0.77)	1.37 (0.74)	1.24 (0.31)	1.29 (1.27)	1.80
E3	0.53 (0.29)	0.41 (0.35)	0.43 (0.21)	0.174 (0.35)	1.10
E4	3.72 (3.44)	1.72 (1.03)	1.79 (4.51)	1.96 (2.20)	2.34
E5	0.69 (0.21)	0.71 (0.43)	0.62 (0.23)	0.76 (0.68)	0.79
E6	1.58 (2.69)	1.21 (2.58)	1.07 (3.50)	1.13 (4.1)	2.47
E7	0.37 (0.13)	0.31 (0.17)	0.34 (0.17)	0.38 (0.19)	0.60
E8	3.15 (4.03)	1.58 (1.00)	1.69 (3.76)	1.62 (2.38)	2.02
E9	6.78 (1.76)	6.94 (2.46)	3.3 (1.87)	4.85 (3.21)	5.89
E10	2.37 (0.53)	2.04 (0.70)	1.8 (0.41)	1.88 (0.77)	3.19

The probability distributions of the calibrated parameters are presented in Figure 5. In both models, the parameter distributions concentrate on narrower ranges when rainfall uncertainty is considered in the calibration. The cumulative distributions of the calibrated parameters present significant differences between the two models, especially the potential infiltration rates of the agricultural and forest soils, and the Manning coefficient of the river (Figure 6). For these parameters, the probability distributions for each hydrological model concentrate at opposite ends of the sampling range. This fact, together with the differences observed in the sensitivities of each model, suggests a limited transferability of calibration results between hydrological models with different spatial structure.

4.3 | Model validation

The performance of the two hydrological models at the validation stage is analogous. The experimental data coverage and the peak discharges obtained with both models are very similar in most of the events (Table 5 and Table 6). The observed discharge data within the

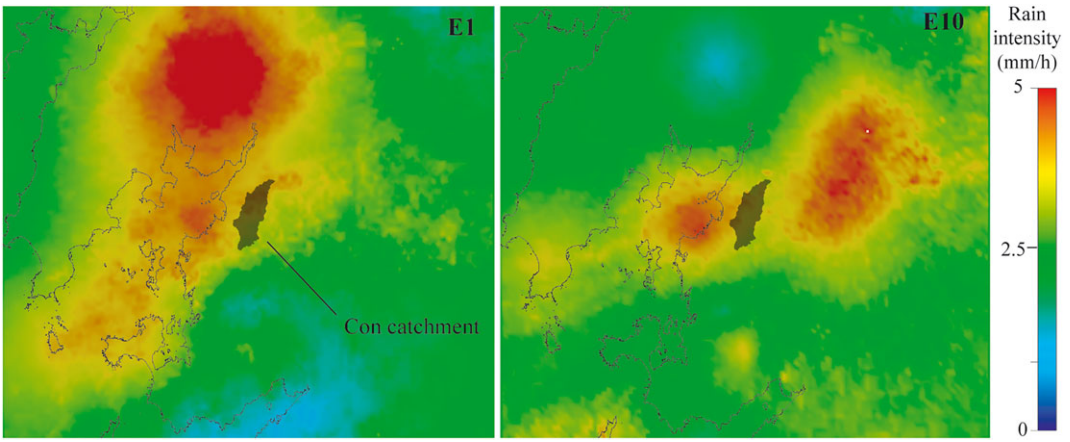

FIGURE 8 Radar measured rain intensities during the peak of the hyetographs of the rain events E1 (left) and E10 (right)

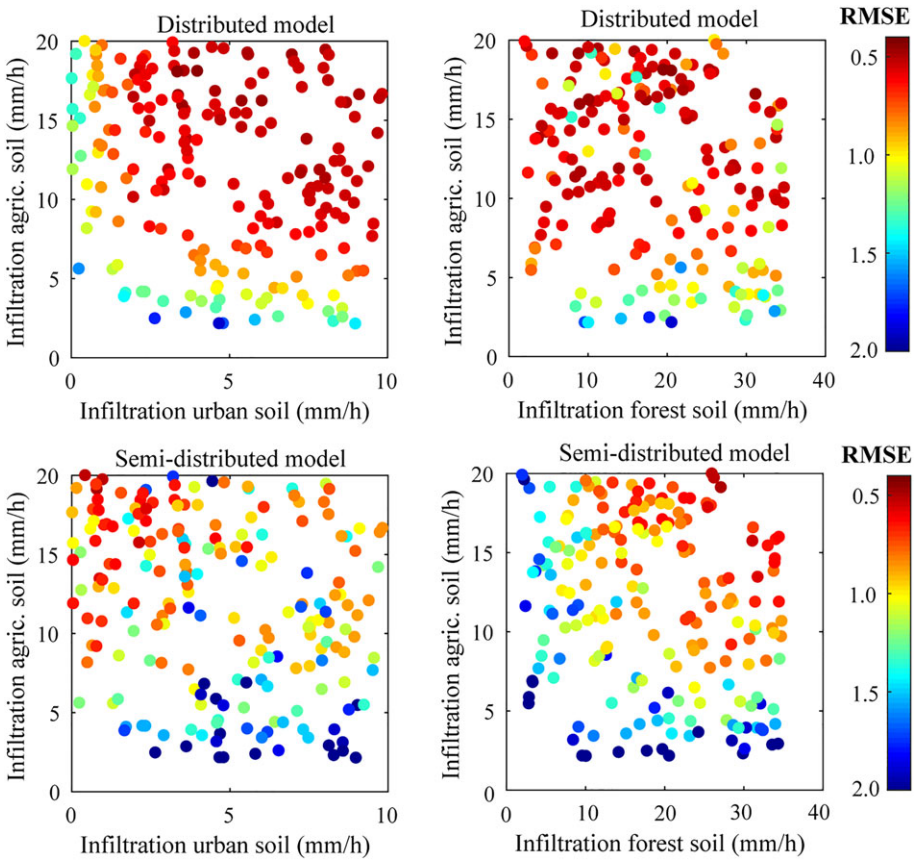

FIGURE 9 Scatter plot of the RMSE for each combination of infiltration rates, computed using the kriged rainfall fields. Results correspond to the averaged values over all the events

95% confidence bounds exceeds 40% in most cases, these being data coverage values common in the validation of hydrological models within the GLUE methodology (Vrugt et al., 2008).

The uncertainty of the discharges predicted in both models is very similar when the same rainfall fields are used as input data (Figure 7). A higher uncertainty of rainfall input results in wider uncertainty bounds on the discharges predicted by both hydrological models. Therefore, in the events in which rainfall data presents highest uncertainties (i.e., event E8 in Table 4), the uncertainty bounds of the predicted discharges are substantially wider.

5 | DISCUSSION

5.1 | Rainfall interpolation and uncertainty quantification

The accuracy of the rainfall predictions obtained with the methodology described in Section 3 varies depending on the type of storm event. In the events that originate from an extended weather system, the spatial correlation of the rainfall is high, and an accurate estimation of the rainfall over the study catchment can be obtained from the nearby rain gauges. Because of this, the hyetographs observed at the validation rain gauges (RG1, RG2, and RG3) are correctly predicted during these events (i.e., E1 and E7). On the contrary, when the weather system is patchy across the study area, as is the case in events E9 and E10 (Figure 8), the spatial correlation of rainfall decreases, and the nearby rain gauges are not capable of accurately capturing the spatial and temporal evolution of the storm. As a result, the interpolated rainfall estimates are worse and do not accurately reproduce the measured values at the validation rain gauges.

Regardless of the spatial structure of the rainfall, the uncertainty of the interpolated fields increases with the rain intensity. This is because, in order to quantify rainfall uncertainty, the conditional simulation technique generates Gaussian error fields that are scaled with the rain intensity. Therefore, higher rain intensities will always result in higher prediction uncertainties. However, these higher rainfall uncertainties do not ensure that the rainfall observed at the validation rain gauges is properly reproduced (Table 4), because it depends whether the spatial structure of the rain event is properly captured or not. Thus, in order to improve rainfall characterization, and consequently discharge predictions, efforts should focus on accurately capturing the weather front evolution, using tools such as meteorological radar and satellite precipitation data. This is especially relevant in catchments located in climatic areas like the ones under study here (those like the Atlantic and U.S. Pacific coasts, for instance), in which the storm events associated with the uplifting of low pressure fronts can result in rainfall with a high spatial and temporal variability.

5.2 | Effects of rain uncertainty on parameter sensitivity and model calibration

The sensitivities and the cumulative distributions of the calibrated input parameters vary significantly between the fully distributed and semidistributed hydrological models. This means that model structure

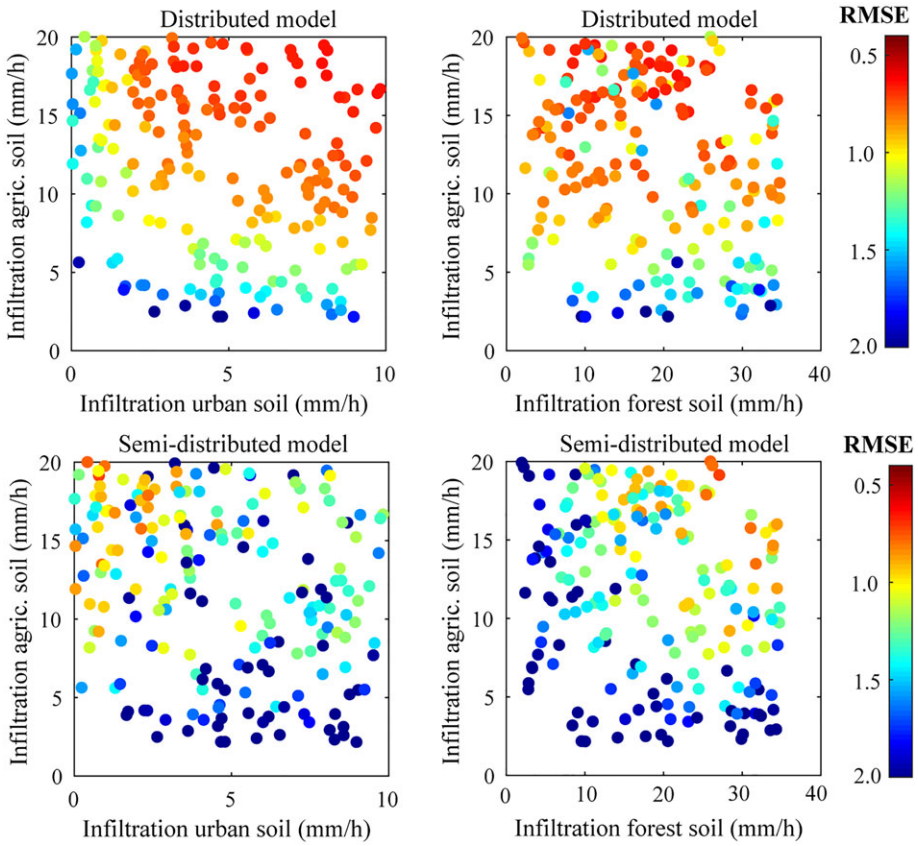

FIGURE 10 Mean bound amplitude (MBA) of the 95% confidence interval of the rainfall and discharge predictions

has an effect on the value of the input parameters, even though both models are physically based and use the same input parameters. This, indeed, has been observed elsewhere (Alvarez-Garreton et al., 2015). However, in both hydrological models the uncertainty of rainfall data has the same effect on the calibration results. When rainfall uncertainty is included in the calibration process, the cumulative distribution of the calibrated input parameters concentrate on narrower ranges.

To understand the reason for this behaviour, the result of the calibration process when the rain uncertainty is not taken into account should first be analysed. Figure 9 represents the RMSE of the simulations performed with different combinations of input parameters, when rainfall uncertainty is not considered in the simulations. The results show that, in both hydrological models, the performance of a specific simulation is determined mostly by two infiltration rates. In the semidistributed model, the infiltration rates that control model performance are those of the agricultural and forest land uses, whereas in the distributed model the most relevant infiltration rates are those of the urban and agricultural soils. This strong equifinality implies that similar model performance can be expected for different combinations of two input parameters. This fact is also reflected in the sensitivities of the two hydrological models.

When rainfall uncertainty is considered in the calibration, the performance of both models is again determined by the same parameters (Figure 10), but in this case, the ranges of infiltration rates that achieve the best performances are much narrower. This is because when

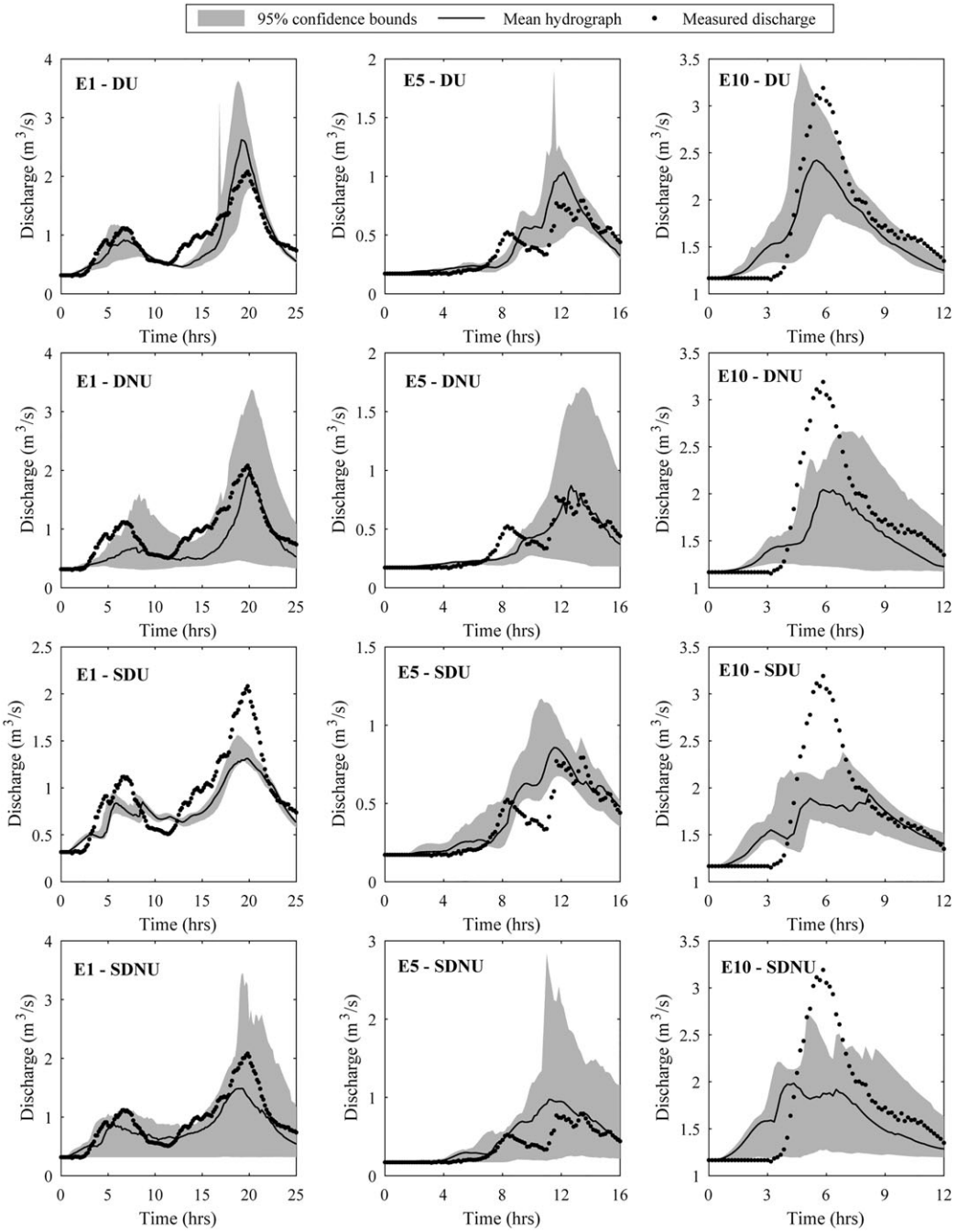

FIGURE 11 Predicted and measured hydrographs at the catchment outlet determined using distributed (D) and semidistributed (SD) models with the rain fields including rainfall uncertainties (U) or without including the predicted rain uncertainty (NU)

rainfall uncertainty is not considered, the input parameters are the only source of uncertainty, and thus they must account for the whole uncertainty in the calibration process. In both models, the inclusion of rainfall uncertainty decreases the equifinality on the calibration and results in cumulative distributions of the input parameters concentrated in narrower ranges.

5.3 | Effects of model structure on the calibration results

As shown in Figure 9 and Figure 10, the parameters that explain the performance of each hydrological model are different for the semidistributed and fully distributed models. Because the spatial distribution of all the land uses is the same in both models, these differences in sensitivity suggest that the role of each land use on the hydrological response of the catchment is different depending on the model structure.

The low sensitivity of the output of the fully distributed model to the Manning coefficient of the river is probably explained by the fact that the inertial terms are more relevant than the frictional terms when the flow propagates along the river network. Because the semidistributed model propagates the flow along the river using the kinematic wave equation, which ignores inertia, the friction terms have to artificially balance the inertial forces. This leads to roughness values of the semidistributed model, which go far beyond the ones recommended in hydraulic reference manuals (Figure 6).

5.4 | Effects of rainfall data on model validation

The performance of the two hydrological models varies substantially from one event to another during the validation stage. In the events in which the kriged hyetographs capture the evolution of the weather front, the discharges computed by both hydrological models correctly reproduce the shape of the observed hydrographs (Events E1 and E5 in Figure 11). By contrast, in the events in which the observed rainfall is not captured properly, the predictions of the hydrological models deteriorate (Event E10 in Figure 11).

In both models, the uncertainty bounds on the discharge predictions decrease when rainfall uncertainty is considered in the calibration, because the equifinality on the input parameters is reduced. Very similar uncertainty bounds on the predicted discharges are obtained with both the semidistributed and the fully distributed models (Figure 7). This implies that a similar propagation of rainfall uncertainty is given by both models, regardless of their spatial discretization.

6 | CONCLUSIONS

A study on the effect of rainfall uncertainty on the performance of physically based fully and semidistributed hydrological models has been presented. It was conducted in a small catchment subject to intense rainfalls with a high spatial and temporal variability.

Results show that rainfall data has a very relevant impact on the accuracy of the discharge predictions performed by both hydrological models. When the estimations of the spatial and temporal evolution of the rainfall fields in the whole catchment are accurate, the discharges computed by both models correctly reproduce the observed hydrographs, and most of the observed discharge data lies within the uncertainty bounds, regardless of whether rainfall uncertainty, is included in the computations or not. By contrast, when the estimated rainfall fields do not correctly capture the peak rain intensity, the computed hydrographs do not reproduce the measured hydrographs. In these latter cases, including the uncertainty of rainfall data has a very limited effect towards improving the accuracy of the discharge predictions, even if rainfall uncertainty is properly characterized.

Very similar uncertainties on the discharge predictions are observed in both hydrological models, which suggests that the uncertainty on discharge predictions is mainly conditioned by the uncertainty of input rainfall data. If rainfall uncertainty is included in model calibration, the calibrated distributions of the input parameters concentrate on narrower ranges, and the equifinality of the input parameters is reduced. This decrease in parameter equifinality also results in narrower confidence bounds of the discharge predictions.

The results presented here underline the importance of improving the accuracy of rainfall data, rather than increasing model complexity, towards effecting positive refinements in the discharge predictions of semidistributed and fully distributed hydrological models.

ACKNOWLEDGMENTS

This study was supported by the Spanish Ministerio de Economía y Competitividad through the CAPRI project (Probabilistic Flood Prediction with High Resolution Hydrologic Models from Radar Rainfall Estimates; Reference CGL2013-46245-R). Ignacio Fraga received financial support from the Xunta de Galicia (Centro Singular de Investigación, Galicia, accreditation 2016–2019) and the European Regional Development Fund. The authors would also like to thank MeteoGalicia (Galician Regional Weather Service) for the rainfall data provided for this study.

ORCID

Ignacio Fraga http://orcid.org/0000-0001-5626-7781

REFERENCES

Alvarez-Garreton, C., Ryu, D., Western, A. W., Su, C. H., Crow, W. T., Robertson, D. E., & Leahy, C. (2015). Improving operational flood ensemble prediction by the assimilation of satellite soil moisture: Comparison between lumped and semi-distributed schemes. *Hydrology and Earth System Sciences*, *19*(4), 1659–1676. https://doi.org/10.5194/hess-19-1659-2015

Arnaud, P., Bouvier, C., Cisneros, L., & Dominguez, R. (2002). Influence of rainfall spatial variability on flood prediction. *Journal of Hydrology*, *260*(1), 216–230. https://doi.org/10.1016/S0022-1694(01)00611-4

Bargaoui, Z. K., & Chebbi, A. (2009). Comparison of two kriging interpolation methods applied to spatiotemporal rainfall. *Journal of Hydrology*, *365*(1–2), 56–73. https://doi.org/10.1016/j.jhydrol.2008.11.025

Bárdossy, A., & Das, T. (2008). Influence of rainfall observation network on model calibration and application. *Hydrology and Earth System Sciences Discussions*, *12*(1), 77–89.

Beven, K., & Binley, A. (1992). The future of distributed models: Model calibration and uncertainty prediction. *Hydrological Processes*, *6*(3), 279–298. https://doi.org/10.1002/hyp.3360060305

Beven, K. J. (2011). *Rainfall-runoff modelling: The primer*John Wiley & Sons.

Bladé, E., Cea, L., Corestein, G., Escolano, E., Puertas, J., Vázquez-Cendón, E., … Coll, A. (2014). Iber: herramienta de simulación numérica del flujo en ríos. *Revista Internacional de Métodos Numéricos Para Cálculo Y Diseño en Ingeniería*, *30*(1), 1–10. https://doi.org/10.1016/j.rimni.2012.07.004

Blasone, R. S., Vrugt, J. A., Madsen, H., Rosbjerg, D., Robinson, B. A., & Zyvoloski, G. A. (2008). Generalized likelihood uncertainty estimation (GLUE) using adaptive Markov Chain Monte Carlo sampling. *Advances in Water Resources*, *31*(4), 630–648. https://doi.org/10.1016/j.advwatres.2007.12.003

Cabalar-Fuentes, M. (2005). Los temporales de lluvia y viento en Galicia. Propuesta de clasificación y análisis de tendencias (1961-2001). Investigaciones Geográficas (Esp), 36.

Cea, L., Bermúdez, M., & Puertas, J. (2011). Uncertainty and sensitivity analysis of a depth-averaged water quality model for evaluation of *Escherichia Coli* concentration in shallow estuaries. *Environmental Modelling & Software*, *26*(12), 1526–1539. https://doi.org/10.1016/j.envsoft.2011.08.001

Cea, L., & Bladé, E. (2015). A simple and efficient unstructured finite volume scheme for solving the shallow water equations in overland flow applications. *Water Resources Research*, *51*(7), 5464–5486. https://doi.org/10.1002/2014WR016547

Cea, L., Fraga, I., Puertas, J., Álvarez, M., Bermúdez, M., Coquerez, S. & Pettazzi, A. (2015). Influencia de la densidad espacial de estaciones pluviométricas y de la disponibilidad de datos radar en los hidrogramas de tormenta calculados con un modelo hidrológico distribuido: Aplicación a una cuenca de 24 Km^2 en el Noroeste de España. *Proceedings of the IV Jornadas de Ingeniería del Agua. 21–22 Octubre 2015*, Córdoba *(España)*.

Cea, L., Legout, C., Darboux, F., Esteves, M., & Nord, G. (2014). Experimental validation of a 2D overland flow model using high resolution water depth and velocity data. *Journal of Hydrology*, *513*, 142–153. https://doi.org/10.1016/j.jhydrol.2014.03.052

Cea, L., Legout, C., Grangeon, T., & Nord, G. (2016). Impact of model simplifications on soil erosion predictions: Application of the GLUE methodology to a distributed event-based model at the hillslope scale. *Hydrological Processes*, *30*(7), 1096–1113.

Ciach, G. J. (2003). Local random errors in tipping-bucket rain gauge measurements. *Journal of Atmospheric and Oceanic Technology*, *20*(5), 752–759. https://doi.org/10.1175/1520-0426(2003)20<752:LREITB>2.0.CO;2

Delrieu, G., Wijbrans, A., Boudevillain, B., Faure, D., Bonnifait, L., & Kirstetter, P. E. (2014). Geostatistical radar–raingauge merging: A novel method for the quantification of rain estimation accuracy. *Advances in Water Resources*, *71*, 110–124. https://doi.org/10.1016/j.advwatres.2014.06.005

Eiras-Barca, J., Brands, S., & Miguez-Macho, G. (2016). Seasonal variations in North Atlantic atmospheric river activity and associations with anomalous precipitation over the Iberian Atlantic Margin. *Journal of Geophysical Research: Atmospheres*, *121*(2), 931–948. https://doi.org/10.1002/2015JD023379

Fraga, I., Cea, L., & Puertas, J. (2017). Validation of a 1D-2D dual drainage model under unsteady part-full and surcharged sewer conditions. *Urban Water Journal*, *14*(1), 74–84. https://doi.org/10.1080/1573062X.2015.1057180

Fleming, M. J., & Doan, J. H. (2009). HEC-GeoHMS geospatial hydrologic modelling extension: User's manual version 4.2. *US Army Corps of Engineers*, *Institute for Water Resources*, *Hydrologic Engineering Centre*, *Davis*, *CA*.

Fraga, I., Cea, L., Puertas, J., Suárez, J., Jiménez, V., & Jácome, A. (2016). Global sensitivity and GLUE-based uncertainty analysis of a 2D-1D dual urban drainage model. *Journal of Hydrologic Engineering*, *21*(5), 04016004. https://doi.org/10.1061/(ASCE)HE.1943-5584.0001335

Fu, S., Sonnenborg, T. O., Jensen, K. H., & He, X. (2011). Impact of precipitation spatial resolution on the hydrological response of an integrated distributed water resources model. *Vadose Zone Journal*, *10*(1), 25–36. https://doi.org/10.2136/vzj2009.0186

García-Feal, O., González-Cao, J., Gómez-Gesteira, M., Cea, L., Domínguez, J., & Formella, A. (2018). An accelerated tool for flood modelling based on Iber. *Water*, *10*(10), 1459. https://doi.org/10.3390/w10101459

Goodrich, D. C., Bums, I. S., Unkrich, C. L., Semmens, D. J., Guertin, D. P., Hernandez, M., … Levick, L. R. (2012). KINEROS 2/AGWA: Model use, calibration, and validation. *Transactions of the ASABE*, *55*(4), 1561–1574. https://doi.org/10.13031/2013.42264

Haberlandt, U. (2007). Geostatistical interpolation of hourly precipitation from rain gauges and radar for a large-scale extreme rainfall event. *Journal of Hydrology*, *332*(1–2), 144–157. https://doi.org/10.1016/j.jhydrol.2006.06.028

Haberlandt, U., & Gattke, C. (2004). Spatial interpolation vs. simulation of precipitation for rainfall-runoff modelling-a case study in the Lippe river basin. In *Hydrology: Science and practice for the 21st century*, edited by: Webb, B., Acreman, M., Maksimovic, C., Smithers, H., and Kirby, C., Proceedings of the British Hydrological Society International Conference (Vol. 1, pp. 120–127).

Habib, E., Krajewski, W. F., & Kruger, A. (2001). Sampling errors of tipping-bucket rain gauge measurements. *Journal of Hydrologic Engineering*, *6*(2), 159–166. https://doi.org/10.1061/(ASCE)1084-0699(2001)6:2(159)

Huard, D., & Mailhot, A. (2006). A Bayesian perspective on input uncertainty in model calibration: Application to hydrological model "abc". *Water Resources Research*, *42*(7), W07416. https://doi.org/10.1029/2005WR004661

Kavetski, D., Kuczera, G., & Franks, S. W. (2006). Bayesian analysis of input uncertainty in hydrological modelling: 2. Application. *Water Resources Research*, *42*(3), W03408. https://doi.org/10.1029/2005WR004376

Kim, D., Kim, H., Pak, G., Jung, M., Mallari, K. J. B., Arguelles, A. C. C., & Yoon, J. (2015). Parameter sensitivity and uncertainty analysis of a stormwater runoff model. *Desalination and Water Treatment*, *54*(13), 3523–3533. https://doi.org/10.1080/19443994.2014.922283

Lebel, T., Bastin, G., Obled, C., & Creutin, J. D. (1987). On the accuracy of areal rainfall estimation: A case study. *Water Resources Research*, *23*(11), 2123–2134. https://doi.org/10.1029/WR023i011p02123

Legates, D. R., & McCabe, G. J. (1999). Evaluating the use of "goodness-of-fit" measures in hydrologic and hydroclimatic model validation. *Water Resources Research*, *35*(1), 233–241. https://doi.org/10.1029/1998WR900018

Lehbab-Boukezzi, Z., Boukezzi, L., & Errih, M. (2016). Uncertainty analysis of HEC-HMS model using the GLUE method for flash flood forecasting of Mekerra watershed, Algeria. *Arabian Journal of Geosciences*, *9*(20), 751. https://doi.org/10.1007/s12517-016-2771-5

Maggioni, V., Vergara, H. J., Anagnostou, E. N., Gourley, J. J., Hong, Y., & Stampoulis, D. (2013). Investigating the applicability of error correction ensembles of satellite rainfall products in river flow simulations. *Journal of Hydrometeorology*, *14*(4), 1194–1211. https://doi.org/10.1175/JHM-D-12-074.1

McMillan, H., Krueger, T., & Freer, J. (2012). Benchmarking observational uncertainties for hydrology: Rainfall, river discharge and water quality. *HydrologicalProcesses*, *26*(26), 4078–4111.

Mei, Y., Nikolopoulos, E. I., Anagnostou, E. N., & Borga, M. (2016). Evaluating satellite precipitation error propagation in runoff simulations of mountainous basins. *Journal of Hydrometeorology*, *17*(5), 1407–1423. https://doi.org/10.1175/JHM-D-15-0081.1

MeteoGalicia. Climatological Reports. Galician Meteorological Agency. Consellería de Medio Ambientee Ordenación do Territorio da Xunta de Galicia. 2017. Available online: http://www.meteogalicia.gal/observacion/informesclima/informesIndex.action?request_locale=gl (accessed on 11July 2018).

Molini, A., Lanza, L. G., & La Barbera, P. (2005). The impact of tipping-bucket raingauge measurement errors on design rainfall for urban-scale applications. *Hydrological Processes*, *19*(5), 1073–1088. https://doi.org/10.1002/hyp.5646

Moulin, L., Gaume, E., & Obled, C. (2009). Uncertainties on mean areal precipitation: Assessment and impact on streamflow simulations. *Hydrology and Earth System Sciences Discussions*, *13*(2), 99–114. https://doi.org/10.5194/hess-13-99-2009

Pan, M., & Wood, E. F. (2009). A multiscale ensemble filtering system for hydrologic data assimilation. Part II: Application to land surface modeling with satellite rainfall forcing. *Journal of Hydrometeorology*, *10*(6), 1493–1506. https://doi.org/10.1175/2009JHM1155.1

Pappenberger, F., & Beven, K. J. (2004). Functional classification and evaluation of hydrographs based on multicomponent mapping (Mx). *International Journal of River Basin Management*, *2*(2), 89–100. https://doi.org/10.1080/15715124.2004.9635224

Pelletier, P. M. (1988). Uncertainties in the single determination of river discharge: A literature review. *Canadian Journal of Civil Engineering*, *15*(5), 834–850. https://doi.org/10.1139/l88-109

Saltelli, A., Ratto, M., Andres, T., Campolongo, F., Cariboni, J., Gatelli, D., … Tarantola, S. (2008). *Global sensitivity analysis. The primer* Chichester, England: John Wiley & Sons.

Scharffenberg, W. A., & Fleming, M. J. (2006). Hydrologic modeling system HEC-HMS: User's manual. US Army Corps of Engineers, Hydrologic Engineering Center.

Shen, Z., Chen, L., Liao, Q., Liu, R., & Hong, Q. (2012). Impact of spatial rainfall variability on hydrology and nonpoint source pollution modeling. *Journal of Hydrology*, *472*, 205–215.

Sobol, I. M. (1998). On quasi-monte carlo integrations. *Mathematics and Computers in Simulation*, *47*(2–5), 103–112. https://doi.org/10.1016/S0378-4754(98)00096-2

Turner, M. R. J., Walker, J. P., & Oke, P. R. (2008). Ensemble member generation for sequential data assimilation. *Remote Sensing of Environment*, *112*(4), 1421–1433. https://doi.org/10.1016/j.rse.2007.02.042

USDA, Soil Conservation Service (1986). Technical Release 55: Urban Hydrology for Small Watersheds. 2nd edn.

Villarini, G., & Krajewski, W. F. (2008). Empirically-basedmodeling of spatial sampling uncertainties associated with rain fall measurements by rain gauges. *Advances in Water Resources*, *31*(7), 1015–1023. https://doi.org/10.1016/j.advwatres.2008.04.007

Villarini, G., Mandapaka, P. V., Krajewski, W. F., & Moore, R. J. (2008). Rainfall and sampling uncertainties: A rain gauge perspective. *Journal of Geophysical Research: Atmospheres*, *113*(D11). https://doi.org/10.1029/2007JD009214

Vischel, T., Lebel, T., Massuel, S., & Cappelaere, B. (2009). Conditional simulation schemes of rain fields and their application to rainfall–runoff modeling studies in the Sahel. *Journal of Hydrology*, *375*(1–2), 273–286. https://doi.org/10.1016/j.jhydrol.2009.02.028

Volkmann, T. H., Lyon, S. W., Gupta, H. V., & Troch, P. A. (2010). Multicriteria design of rain gauge networks for flash flood prediction in semiarid catchments with complex terrain. *Water Resources Research*, *46*(11). https://doi.org/10.1029/2010WR009145

Vrugt, J. A., TerBraak, C. J., Clark, M. P., Hyman, J. M., & Robinson, B. A. (2008). Treatment of input uncertainty in hydrologic modeling: Doing hydrology backward with Markov chain Monte Carlo simulation. *Water Resources Research*, *44*(12). https://doi.org/10.1029/2007WR006720

Zhao, D., Chen, J., Wang, H., & Tong, Q. (2012). Application of a sampling based on the combined objectives of parameter identification and uncertainty analysis of an urban rainfall-runoff model. *Journal of Irrigation and Drainage Engineering*, *139*(1), 66–74.

Zheng, F., Maier, H. R., Wu, W., Dandy, G. C., Gupta, H. V., & Zhang, T. (2018). On lack of robustness in hydrological model development due to absence of guidelines for selecting calibration and evaluation data: Demonstration for data-driven models. *Water Resources Research*, *54*(2), 1013–1030. https://doi.org/10.1002/2017WR021470